Journal of Asian Earth Sciences 200 (2020) 104492

Contents lists available at ScienceDirect

Journal of Asian Earth Sciences

journal homepage: www.elsevier.com/locate/jseaes

Seismic evidence for influences of deep fluids on the 2019 Changning *Ms* 6.0 earthquake, Sichuan basin, SW China

Bing Zhang[a,b], Jianshe Lei[b,*], Guangwei Zhang[b]

[a] Institute of Geophysics, China Earthquake Administration, Beijing 100081, China
[b] Key Laboratory of Crustal Dynamics, Institute of Crustal Dynamics, China Earthquake Administration, Beijing 100085, China

ARTICLE INFO

Keywords:
Double-difference tomography
Seismic velocity
Earthquake relocation
Changning earthquake
Earthquake mechanism

ABSTRACT

An *Ms* 6.0 earthquake struck Changning county, Sichuan basin, SW China on 17 June 2019, which caused huge casualties and economic losses. Four *Ms* greater than 5.0 events subsequently occurred around the Changning source area, three of which occurred within one week. In order to better understand the mechanism of these moderate-sized earthquakes, we determine 3-D high-resolution velocity models around the source area simultaneously relocating earthquakes using double-difference tomography. In the present study, we use a total of 53,487 P-wave and 52,527 S-wave arrival times from 8818 events recorded at 39 seismic stations. Our results show that focal depths of the Changning mainshock and most aftershocks are ~5–10 km, and they form a fault plane with a steep dip angle. Most earthquakes are underlain by the zone with low Vp, low Vs, and high Vp/Vs anomalies, reflecting the existence of fluids there. These results suggest that the Changning mainshock and other moderate-sized earthquakes might be associated with the influence of fluids that could decrease effective normal stress on the fault planes. These fluids might be related to the hot and wet mantle upwelling in the big mantle wedge due to the deep subduction of the Indian plate down to the mantle transition zone. A clear high-to-low velocity transition zone is observed at ~10 km depth beneath the Gongxian and Xingwen swarms, which matches well with the detachment layer revealed by deep seismic soundings in the area. All these results suggest that the structural contrast could control the mainshock generation and aftershock extension.

1. Introduction

On 17 June 2019, an *Ms* 6.0 earthquake struck Changning country, southern margin of the Sichuan basin, Southwestern China (Fig. 1). The China Earthquake Networks Centre reported that the epicenter was located at 28.34°N, 104.90°E with a focal depth of 16 km, approximately 269 km southeast of Chengdu city in the Sichuan basin (Fig. 1). The devastating earthquake caused severe losses of lives and properties. Furthermore, aftershocks lasted for more than one week, and there had been a total of 202 aftershocks with magnitude larger than 2.0, including 4 *Ms* ≥ 5.0, 5 *Ms* 4.0–4.9, and 46 *Ms* 3.0–3.9 aftershocks till 4 July 2019 (http://www.cea.gov.cn/cea/dzpd/index.html).

The Changning source area (104°E-105.5°E, 27.7°N-28.9°N), situated in the southeast segment of North-South Seismic Belt, is located on the trip junction of the Sichuan basin, Sichuan-Yunnan block, and Yangtze block (Fig. 1). Under the far distance stress influence from the Songpan-Ganzi block to the northwest and the Sichuan-Yunnan block to the west, as well as the extrusion-uplifting actions from the Sichuan basin to the north and the Yangtze block to the south, the study area has being become one of the most seismically hazard areas in recent years (e.g., Deng et al., 2002; Xu et al., 2016; Fan et al., 2018; He et al., 2011; Lei et al. 2019a,b). Around the study area, many large earthquakes occurred recently, such as the 2008 Wenchuan *Ms* 8.0 earthquake and 2013 Lushan *Ms* 7.0 earthquake on the Longmenshan fault zone to the northwest (e.g., Lei and Zhao, 2009; Lei et al., 2014; Deng et al., 2014; Pei et al., 2010) and the 2014 Ludian *Ms* 6.5 earthquake on the Zhaotong-Ludian fault to the south (e.g., Fang et al., 2015; Zhang et al., 2014; Xie et al., 2015) (Fig. 1), in addition to the 8 August 2017 Jiuzhaigou *Ms* 7.0 earthquake on the easternmost edge of the Kunlunshan fault (e.g., Liang et al., 2018; Tung et al., 2019). Such a study area is located in the big mantle wedge (BMW) formed by the deep subduction and long-term stagnancy of the Indian plate in the mantle transition zone (e.g., Lei et al., 2009; Lei et al. 2019a; Lei and Zhao, 2016).

In such a small-scale tectonic unit of the Changning source area, geological features are very complicated, which are mainly controlled by the co-existence of the NE-SW and NW-SE oriented faults characterized by multi-stage activities (e.g., Deng et al., 2002; Xu et al.,

* Corresponding author.
E-mail address: jshlei_cj@126.com (J. Lei).

https://doi.org/10.1016/j.jseaes.2020.104492
Received 26 March 2020; Received in revised form 7 July 2020; Accepted 7 July 2020
Available online 12 July 2020

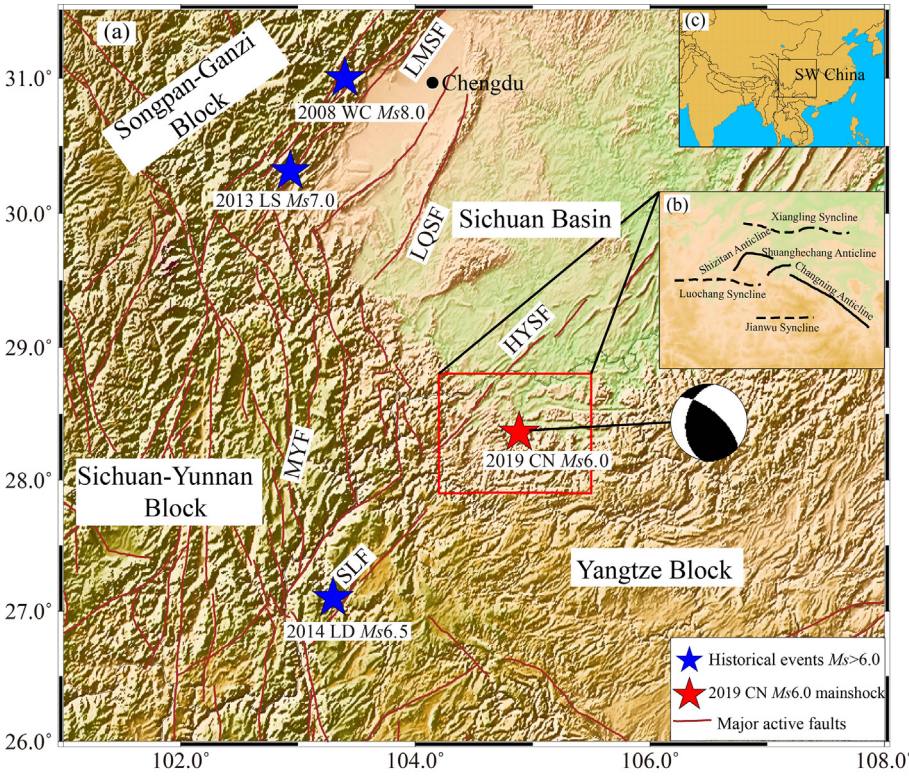

Fig. 1. (a) A map of major tectonics in the study area. Blue stars represent earthquakes with magnitudes greater than 6.0 that occurred around the study area in recent decades, including the 2008 Wenchuan *Ms* 8.0 earthquake (2008 WC *Ms* 8.0), 2013 Lushan *Ms* 7.0 earthquake (2013 LS *Ms* 7.0), and 2014 Ludian *Ms* 6.5 earthquake (2014 LD *Ms* 6.5), respectively. The red star denotes the 2019 Changning *Ms* 6.0 mainshock (2019 CN *Ms* 6.0). The beach ball shows focal mechanism solution of 2019 Changning *Ms* 6.0 mainshock (Liang et al., 2020). Brown solid lines denote major active faults (Deng et al., 2002). LMSF, the Longmenshan fault zone; LQSF, the Longquanshan fault; MYF, the Mabian-Yanjin fault; SLF, the Shaotong-Ludian fault; HYSF, the Huayingshan fault. **(b)** Major geological settings around the 2019 Changning *Ms* 6.0 mainshock. Black solid lines denote major anticlines, while black dashed lines are major synclines (Yi et al., 2019). **(c)** Location of the study area. (For interpretation of the references to color in this figure legend, the reader is referred to the web version of this article.)

2016; Fan et al., 2018; He et al., 2011; He et al., 2019). As the major structural elements of the earthquake source area, the NW-SE Changning anticline is the narrowest in the Xuyong area and becomes wider northwestward when it passes through Gongxian and Gaoxian (He et al., 2011; He et al., 2019). Moreover, the anticline slightly bends southwestward in the northwest terminal (He et al., 2011; He et al., 2019). Along the Changning anticline, a series of secondary faults and related folds were generated due to the axis plane fracturing, where an east-west oriented band-like shape extends with a mosaic distribution of anticlines and synclines from the north to the south including Xiangling syncline, Shizitan anticline, Shuanghechang anticline, Changning anticline, Luochang syncline, and Jianwu syncline in and around the Changning source area (Fig. 1). Meanwhile, the Cambrian, Ordovician, Silurian, Permian, Triassic and Jurassic strata are well exposed sequentially from the nucleus to the periphery of the Changning anticline (He et al., 2019; Wang et al., 2015). In recent years, with the rapid development of shale gas production and hydraulic fracturing studies close to the Changning earthquake, the study area of interests remains seismically active (Fig. 2a). Less than 20 km south away from the Changning mainshock, an *Ms* 5.7 earthquake occurred in Xingwen on 16 December 2018 and an *Ms* 5.3 earthquake followed in Gongxian on 3 January 2019 (Fig. 2b; Lei et al., 2017; Lei et al. 2019b). Till 4 July 2019, four moderate-sized strong earthquakes ($Ms > 5.0$) occurred in the area after the 17 June 2019 Changning mainshock (Yi et al., 2019; Long et al., 2020). The generation mechanism of these earthquakes still remains debated, and social public and local government have raised extensive concerns on it.

To better understand the mechanism of the 2019 Changning *Ms* 6.0 mainshock and moderate-sized aftershocks, we present 3-D high-resolution P-wave (Vp) and S-wave (Vs) velocity models around the study area using the double-difference seismic tomography (Zhang and Thurber, 2003; Zhang et al., 2009) by a large number of P- and S-wave arrival times recorded at 39 China Earthquake Administration stations from 1 December 2018 to 4 July 2019. Our models provide new lights on the generation mechanism of the Changning earthquake sequences.

2. Data and method

In this study, we adopt the double-difference tomography method (Zhang and Thurber, 2003; Zhang et al., 2009) for velocity inversion and earthquake relocation. In addition to absolute arrival times, differential times between pairs of earthquakes are also used to get high-resolution Vp and Vs structures as well as earthquake locations. By taking differences between travel times of nearby event pairs, the errors outside the source area with similar ray paths can be largely reduced, and thus the structure near the Changning source area can be reasonably resolved. Additional details of this method can be found in Zhang and Thurber (2003).

In the present study, we collect earthquakes that were recorded at more than 6 seismic stations. Because we are mainly concerned about the velocity structure around the 2019 Changning source area, we choose only the arrival times with epicentral distances shorter than 250 km. Finally, a total of 39 stations (Fig. 2a) and 8818 earthquakes from 1 December 2018 to 4 July 2019 (Fig. 2), including 53487 P-wave and 52,527 S-wave absolute travel times (Fig. 3a), are selected in the present study. The gap angles of the selected stations are less than 30° (Fig. 2a), indicating good azimuthal coverage of seismic stations to obtain high-quality earthquake relocations and tomographic images. In addition, there are ten seismic stations with epicentral distance less than 50 km (Fig. 2b), indicating a strong constrain on focal depth. To obtain the double difference data, we set a maximum distance between event pairs to 4 km. The center of the coordinate system is set up at the point of 28.3°N and 104.8°E and grid spacing of 0.1° × 0.1° in the X and Y directions (Fig. 2b) is used in the inversion. In the Z direction, the layer depth is positioned at depths of 0, 2, 4, 7, 10, 14, 18, and 38 km. The starting 1-D velocity model (Fig. 3b) is constructed using previous results (Lei et al. 2019b; Zhang et al., 2014). The 3-D Vp and Vs models and earthquake relocations are jointly inverted through ten iterations. In consequence, we obtain 6833 relocated earthquakes, which have the average relative errors of 0.161 km in latitude, 0.157 km in longitude and 0.249 km in depth, respectively. The root-mean-square travel-time residual is significantly reduced from 0.17 s before to 0.04 s after the

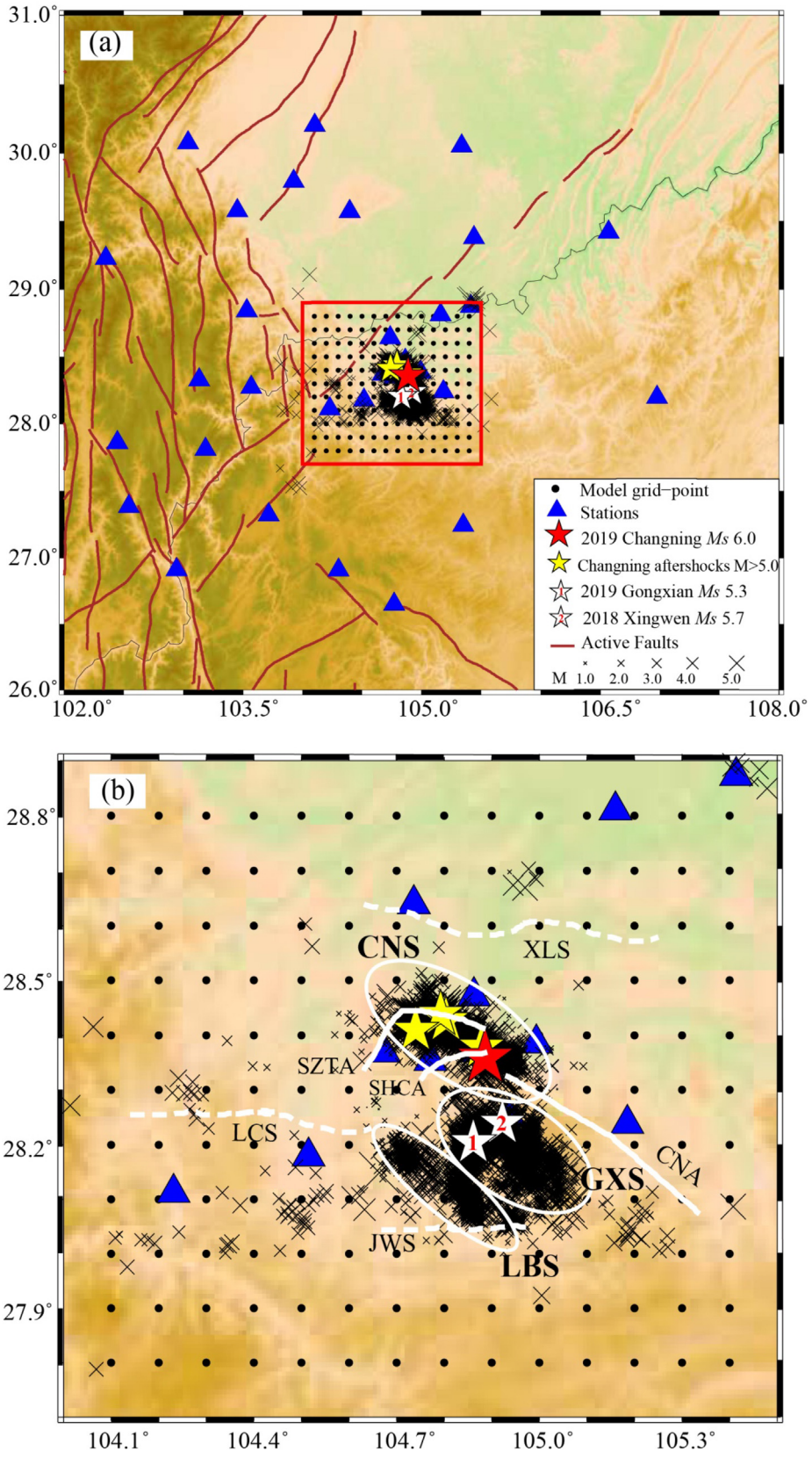

Fig. 2. (a) Distribution of seismic stations (blue triangles) and events (black crosses) used in the present study. The red star represents the 2019 Changning *Ms* 6.0 mainshock, and the yellow stars denote the recent aftershocks with magnitudes greater than 5.0, whereas white stars numbered 1 and 2 are the 2019 *Ms* 5.3 Gongxian and the 2018 *Ms* 5.7 Xingwen earthquake, respectively. Black dots are the grid-points that are set in the model. Brown solid lines denote major active faults in the study area (Deng et al., 2002). **(b)** The magnified Changning source area in the present study, which is framed by the red lines in (a). All the events are roughly divided into three swarms by the white ellipses, Changning swarm (CNS), Gongxian and Xingwen swarms (GXS), Luobiao swarm (LBS), respectively. White solid lines denote Changning anticline (CNA), Shuanghechang anticline (SHCA), and Shizitan anticline (SZTA), whereas white dotted lines are Jianwu syncline (JWS), Luochang syncline (LCS), and Xiangling syncline (XLS) (Yi et al., 2019). Other symbols are the same as in (a). (For interpretation of the references to color in this figure legend, the reader is referred to the web version of this article.)

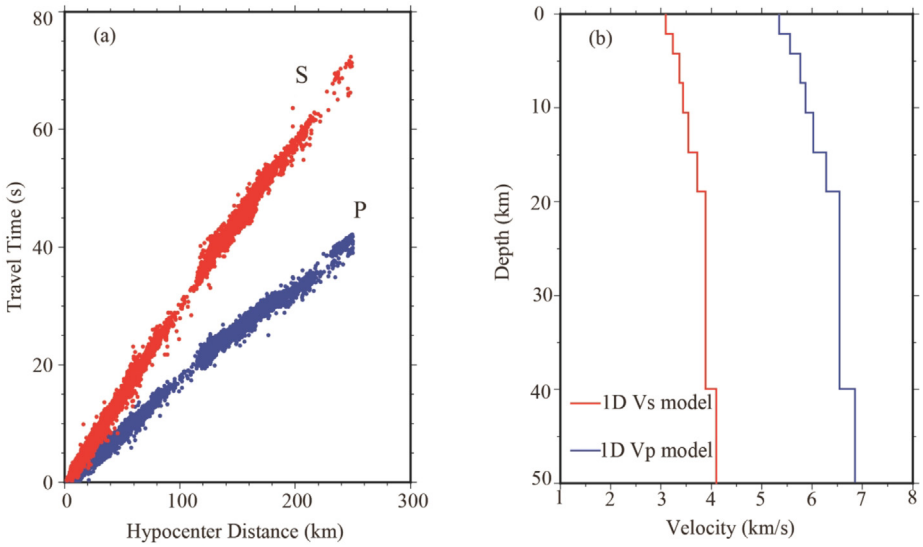

Fig. 3. (a) Observed travel times (in second) versus epicentral distances (in km) for P- wave (blue dots) and S-wave (red dots). **(b)** The initial 1-D P- (blue line) and S- wave (red line) velocity models, which are constructed from previous studies (e.g., Lei et al. 2019b; Zhang et al., 2014), adopted for the 3-D tomographic inversions. Vp/Vs is fixed to be 1.73. (For interpretation of the references to color in this figure legend, the reader is referred to the web version of this article.)

inversion. The Vp/Vs ratio is directly obtained by dividing Vp by Vs in the same grid node in the models (Zhang et al., 2009; Guo et al., 2018).

3. Results

3.1. Resolution analyses

To examine the ray coverage in the study area and the resolution scale of our tomographic model, we perform many checkerboard resolution tests by adopting different grid intervals. Due to the scope of the paper, here we only show the test results for Vp and Vs velocity models with grid intervals of 0.15° × 0.15° and 0.10° × 0.10° in the horizontal directions and at depth layers of 2, 4, 7, 10, 14 and 18 km (Fig. 4). Alternatively negative and positive velocity anomalies of up to 6% are assigned to the 3-D grid nodes in the modeling space in the initial model. Random noise with zero mean and a standard deviation of 0.2 s is added to the synthetic P- and S-wave travel times to account for data errors. Output models are obtained through inversions of the synthetic data as the same number of seismic stations, earthquakes and ray paths used in the real data set. By comparing the inverted and input images of the checkerboard model, it is easy to understand where the resolution is good and where it is poor.

We express our output models using the ratio way (Lei and Zhou, 2002; Lei and Zhao, 2005, 2007) by dividing the amounts of inverted velocity anomalies by those in the initial models. Hexagons denote the grid nodes where the pattern of the input velocity anomalies is correctly recovered after the inversion, that is, fast anomalies in the input model are recovered to be fast, and slow ones in the input model are recovered to be slow after the inversion. The size of the hexagon denotes the ratio of the inverted amplitude of the velocity anomaly to the value of the input velocity anomaly. The grid nodes with 100% values are thought to be recovered perfectly. From Fig. 4, we can see that, except for Vp model at 18 km depth and Vs model at 7 and 18 km depths, both Vp and Vs velocity anomalies are generally recovered in the model with grid spacing of 0.15°×0.15°. Although the anomalies of both Vp and Vs models with grid spacing of 0.10° × 0.10° in the horizontal directions are not completely recovered, those around the Changning, Gongxian and Xingwen and Luobiao swarms are generally retrieved (Fig. 4).

To further understand the advantage of the ratio way, here we show an example for comparing two ways to present the results of the checkerboard resolution tests along two vertical cross sections parallel and perpendicular to the Changning swarm (Fig. 5). One is the conventional way as shown in Fig. 5(c, d, g, h), in which open and solid circles show slow and fast velocity anomalies in the output models. However, sometimes it is uneasy to discern if the checkerboard pattern is recovered correctly or not, in particular, for the marginal parts of the study area. Thus, we adopt the ratio way (Fig. 5e, f, i, j; Lei and Zhou, 2002; Lei and Zhao, 2005), which is the same as that in Fig. 4. After comparison, it can easily be seen from Fig. 5(e, f, i, j) that, except for the areas on the margins of the models having lower resolution, the Changning source area shows much high resolution. In particular, for the cross section along the Changning swarm having an implicated pattern of velocity anomalies in the input model (Fig. 5a), the ratio way is much easier to judge where the grid nodes are recovered correctly (Fig. 5e, i). These results suggest that the main structural features around the Changning source area are reliable, which enable us to discuss the mechanism of the 2019 Changning mainshock and moderate-sized aftershocks.

3.2. Tomographic images

Fig. 6 shows our relocated earthquakes (see Appendix A in the Supplementary Interactive Plot Data) and tomographic images of Vp, Vs and Vp/Vs (see Appendix B in the Supplementary Interactive Plot Data) in map view. All relocated earthquakes are mainly focused on the anticlines and synclines. The Changning swarm is located around the Shizitan, Shuanghechang, and Changning anticlines, and the Gongxian and Xingwen swarms are closely related to the Luochang syncline, whereas the Luobiao swarm is associated with the Jianwu syncline. Our Vp, Vs and Vp/Vs models show strong lateral heterogeneities around the 2019 Changning source area (Fig. 6). At 2–4 km depths, the Changning swarm occurred in the zones with low Vs and low Vp/Vs and in the transition zone of high-to-low Vp anomalies, whereas the Gongxian, Xingwen, and Luobiao swarms occurred in low Vp, high Vs and low Vp/Vs anomalies (Fig. 6a, b, g, h, m, n). At 7–10 km depths, the Changning, Gongxian, Xingwen, and Luobiao swarms are all located in the zones with low Vp, high Vp and low Vp/Vs anomalies (Fig. 6c, d, i, j, o, p). At 14–18 km depths, all these swarms are situated in the zone with a complicated pattern of anomalies, but the zones mainly illustrate obvious low Vp, high Vs, and high Vp/Vs anomalies (Fig. 6e, f, k, l, q, r).

To better understand the mechanism of the 2019 Changning mainshock and moderate-sized aftershocks, we plot several vertical cross-sections (Figs. 7-9). Cross sections AA' and BB' passing through the Changning swarm are parallel and perpendicular to the trend of the Changning anticline, respectively (Fig. 7). The earthquake hypocenters are generally located within a narrow zone with low Vp, high Vs and low Vp/Vs northwestward extending from the shallow (at ~2 km depth) crust beneath the Changning arch core to the middle-lower (at

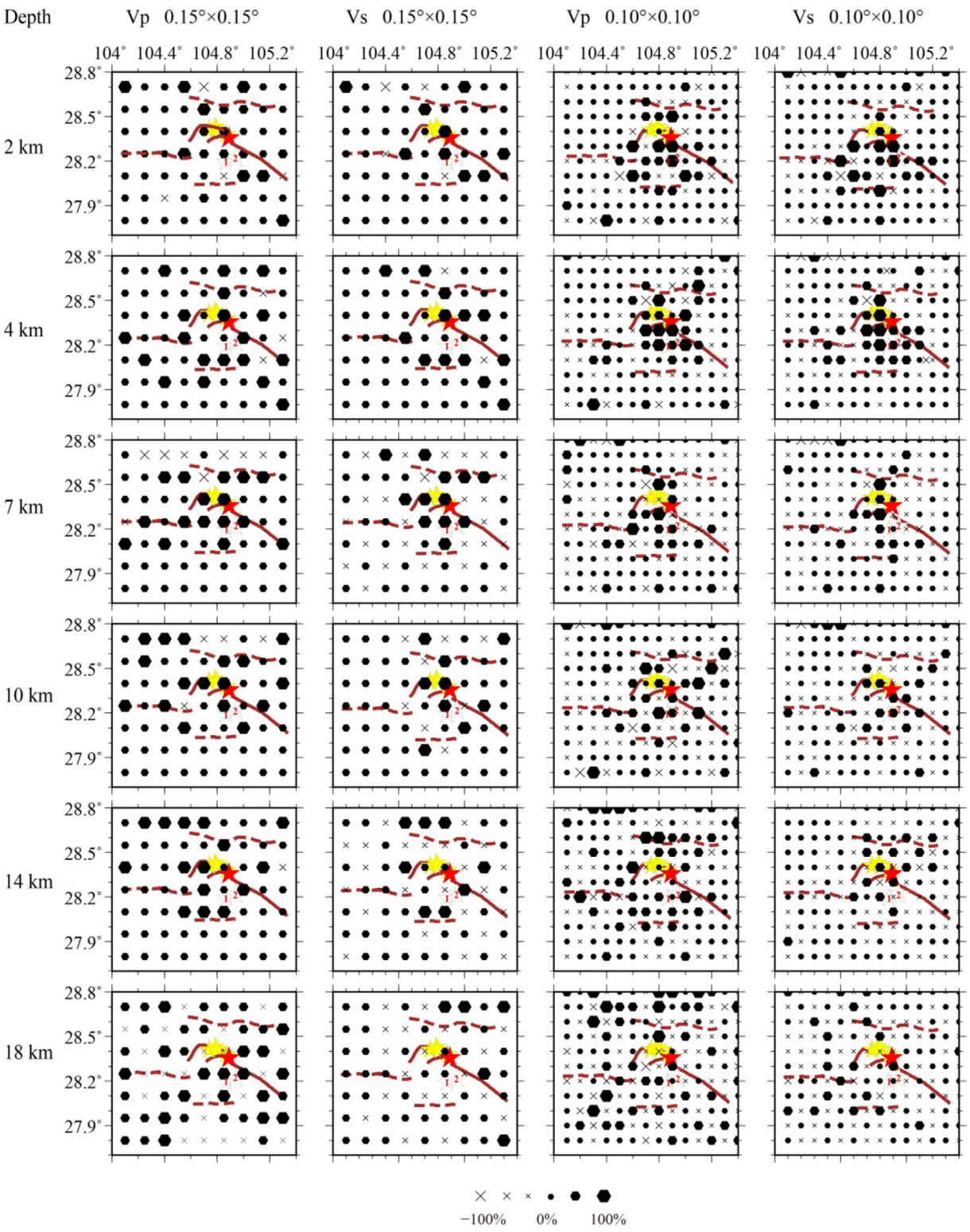

Fig. 4. Results of Vp and Vs checkerboard resolution tests in map view. In the input model, the velocity anomaly is set to ± 6%, relative to the initial 1-D velocity model as shown in Fig. 3b. The first and second columns show Vp and Vs output models with grid spacing of 0.15° × 0.15° in the horizontal directions, whereas the third and fourth columns show the models with grid spacing of 0.10° × 0.10° in the horizontal directions. Depth intervals are shown on the left. Hexagons and crosses denote the grid nodes where the checkerboard pattern is recovered correctly and wrongly, respectively. The hexagons with values of 100% show the grid nodes where the checkerboard pattern is recovered perfectly. The scale for the degree of recovery is shown at the bottom. The red star represents the 2019 Changning *Ms* 6.0 mainshock, and yellow stars denote recent aftershocks with magnitudes greater than 5.0, whereas white stars numbered 1 and 2 are the 2019 *Ms* 5.3 Gongxian and 2018 *Ms* 5.7 Xingwen earthquakes, respectively. Brown solid lines denote major anticlines, whereas brown dotted lines are major synclines (Yi et al., 2019). (For interpretation of the references to color in this figure legend, the reader is referred to the web version of this article.)

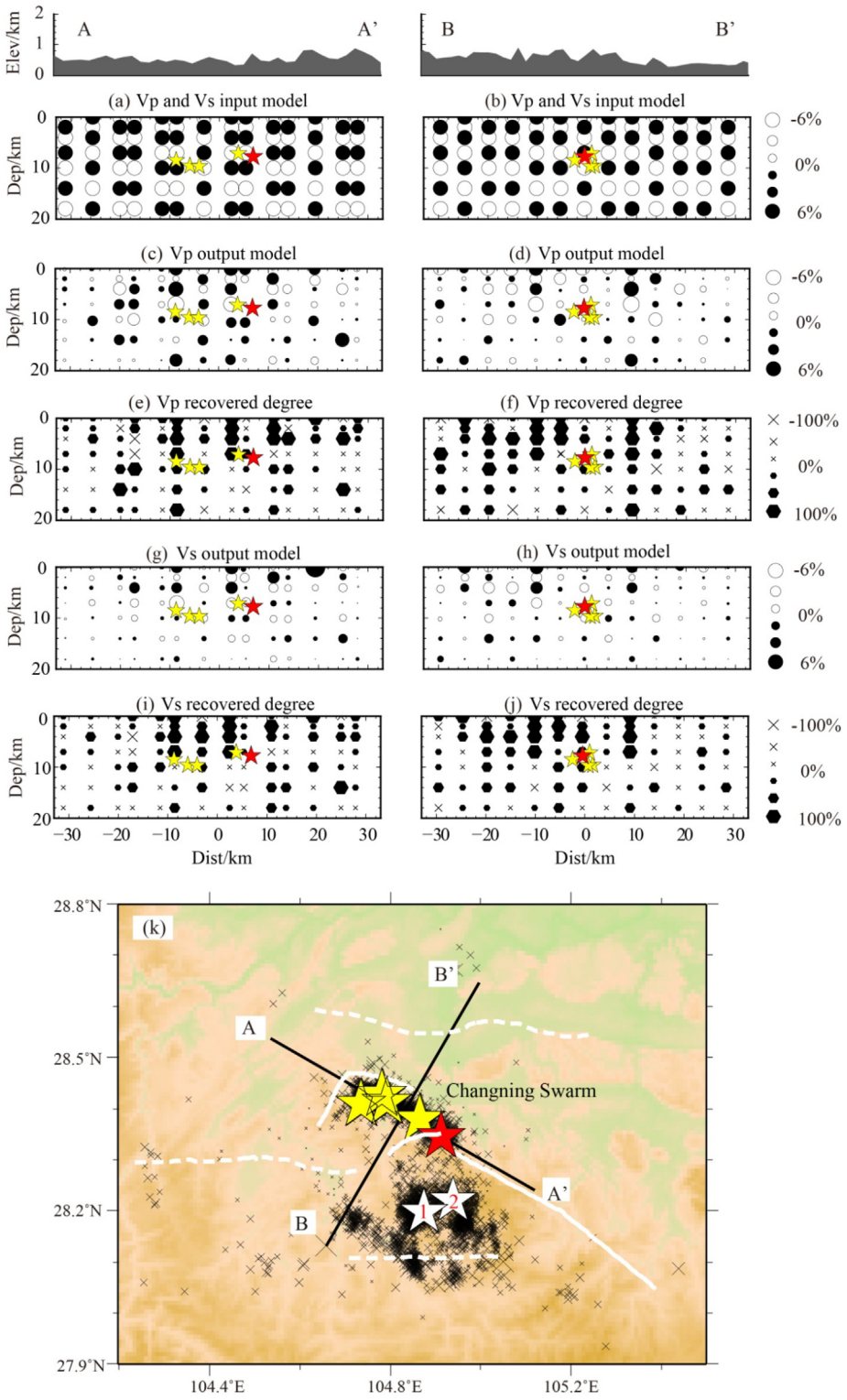

Fig. 5. Results of a checkerboard resolution test for Vp and Vs along cross-sections AA' and BB'. The topography is shown on the top. **(a, b)** Vp and Vs input models with grid spacing of 0.10° × 0.10° in the horizontal directions, respectively. Open and solid circles show slow and fast velocity anomalies with ± 6% perturbations at the grid nodes, the scale of which is shown on the right of (b). **(c, d)** Vp output models. Open and solid circles show the inverted results of slow and fast velocity anomalies at the grid nodes after the inversion. The velocity perturbation scale is shown on the right of (d). **(e, f)** The same as (c, d) but for recovery degree of Vp anomalies. Hexagons and crosses denote the grid nodes where the checkerboard pattern is recovered correctly and wrongly, respectively. The hexagons with values of 100% show the grid nodes where the checkerboard pattern is recovered perfectly, and the crosses with values of −100% show the grid nodes where the checkerboard pattern is not recovered completely. The scale for the degree of recovery is shown on the right of (f). **(g, h)** The same as (c, d) but for Vs. **(i, j)** The same as (e, f) but for Vs. Locations of cross-sections are shown at (k). Other symbols are the same as those shown in Figs. 1 and 2.

~20 km depth) crust beneath the Shuanghechang and Shizitan anticlines, which is well consistent with the extension direction of the Changning moderate-sized aftershocks (Fig. 7a-c). However, a high Vs and low Vp/Vs anomaly appears around the Changning swarm along and across the Changning anticline (Fig. 7b, c, e, f). As shown in Fig. 7d-f, most relocated earthquakes can be identified as a nearly vertical distribution, which is highly consistent with the focal mechanism solution, suggesting that the seismogenic fault of Changning mainshock has a high dip with a predominantly NW-SE oriented strike-slip component simultaneously having a minor left-lateral thrust (Fig. 1; Liang et al., 2020). Cross sections CC' and DD' pass through the Gongxian and Xingwen swarms, and most of the earthquakes occurred in the zone with low Vp, high Vs, and low Vp/Vs anomalies (Fig. 8). It should be noted that both low Vp and Vs discontinuities are observed at 10–15 km depths, which match well with the detachment layer geometrically revealed by the previous seismic sounding profile across the Gongxian and Xingwen swarms (He et al., 2019). Cross section EE' passes through the Luobiao swarm, which illustrates that most

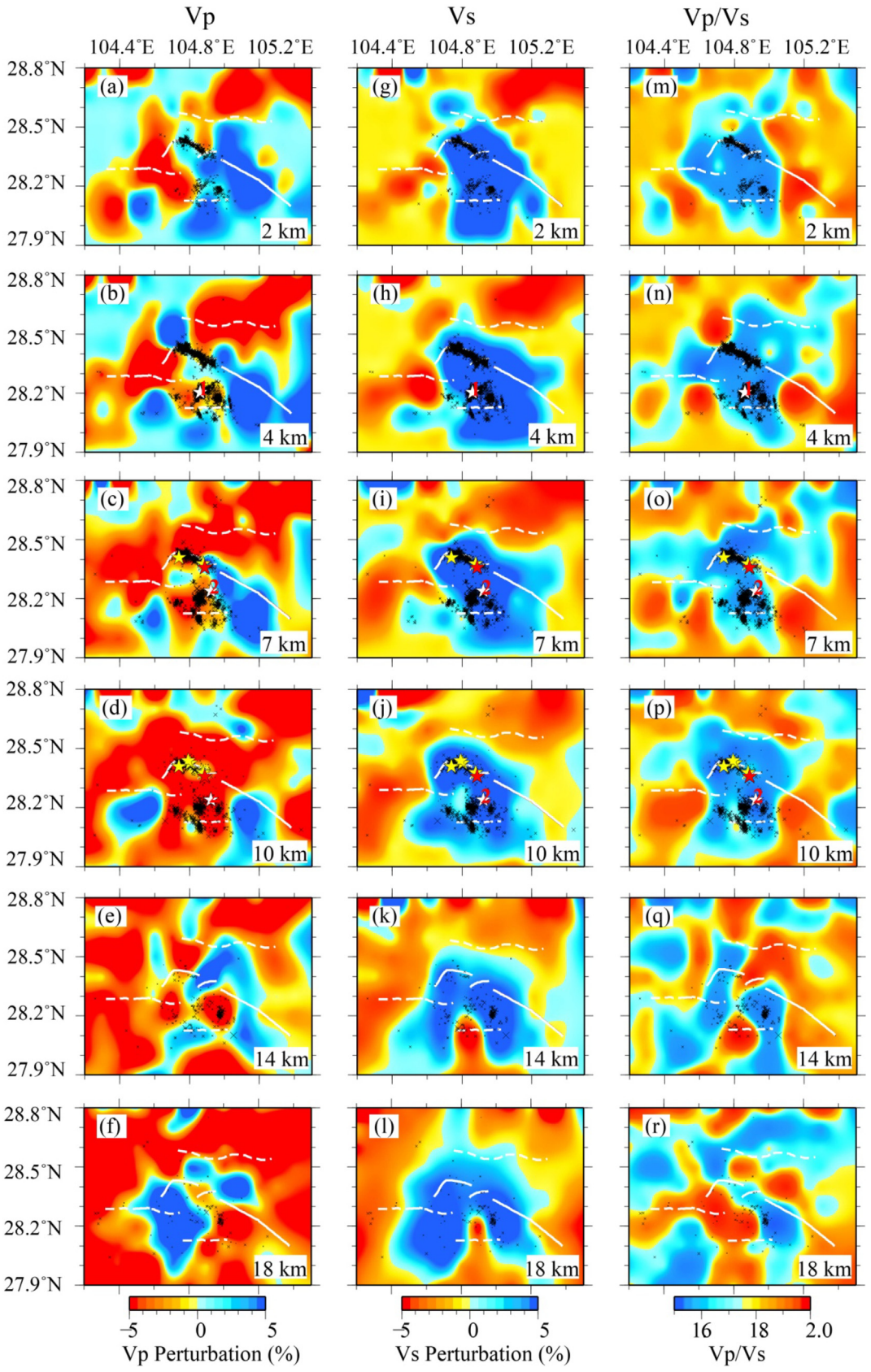

(caption on next page)

Fig. 6. Tomographic images of Vp (the first column) and Vs (the second column) and Vp/Vs (the third column) around the Changning source area at different depths in map view. Depth values are shown at the bottom-right corner of each panel. Vp and Vs are shown as velocity perturbations, relative to the initial velocity models as shown in Fig. 3b. The red color denotes low Vp, low Vs, and high Vp/Vs, respectively, whereas the blue color denotes high Vp, high Vs, and low Vp/Vs, respectively. Their scales are shown at the bottom. Black dots denote relocated small earthquakes that occurred in a range of 2 km depth above and below each layer. The red star represents the 2019 Changning *Ms* 6.0 mainshock, and yellow stars denote recent aftershocks with magnitudes greater than 5.0, whereas white stars numbered 1 and 2 are the 2019 *Ms* 5.3 Gongxian and 2018 *Ms* 5.7 Xingwen earthquakes, respectively. White solid lines denote major anticlines, whereas white dashed lines are major synclines (Yi et al., 2019). (For interpretation of the references to color in this figure legend, the reader is referred to the web version of this article.)

earthquakes occurred at 2–12 km depths in an NW-SE direction cluster with low Vp, high Vs and low Vp/Vs anomalies (Fig. 9). Nevertheless, it can be seen from Figs. 7–9 that all the swarms, including the Changning, Gongxian, Xingwen, and Luobiao swarms and moderate-sized aftershocks, occurred in the zone with low Vp, high Vs, and low Vp/Vs anomalies, but they are underlain by the zone with low Vp, low Vs and high Vp/Vs anomalies.

4. Discussion

Our present results clearly show that the source area of the Changning mainshock and moderate-sized aftershocks are underlain by the anomalous zone with low Vp, low Vs and high Vp/Vs features below 10 km depth (Figs. 6–9). These anomalies possibly indicate the existence of a fluid-filled fractured rock matrix (Mishra et al., 2008; Singh et al., 2012), which may have contributed to the initiation of the Changning mainshock and moderate-sized aftershocks. Such a similar structure could also be detected under other hypocenters in the world, such as the 17 January 1995 Kobe earthquake (M 7.2) in Japan, the 26 January 2001 Bhuj earthquake (M 7.6) in India, and the 28 July 1976 Tangshan (M 7.8) and 12 May 2008 Wenchuan (M 8.0) earthquakes in China (e.g., Zhao et al., 1996; Mishra and Zhao, 2003; Mishra et al., 2008; Lei et al., 2008; Lei and Zhao, 2009). Such an anomalous zone could be related to the influence of fluids that may affect the long-term structural and compositional evolution of the fault zone, change the strength of the fault zone, and alter the local stress regime (Sibson, 1992; Hickman et al., 1995). These influences could have enhanced stress concentration in the seismogenic layer leading to mechanical failure and the nucleation of these earthquakes. Another possibility is that when fluids enter the fault zone, they may decrease the effective normal stress across the fault planes to trigger the earthquakes (e.g., Bruhn and Schultz, 1996; Lei and Zhao, 2009).

In addition to the lower crustal channel flow (e.g., Royden et al., 1997; Royden et al., 2008), there could be several other sources of fluids in the crust, such as the dehydration of hydroxyl-bearing minerals in the crust, fluids trapped in pore spaces, and meteoric water (e.g., Zhao et al., 2002; Lei et al., 2012) as well as the water injection in the Changning salt mine area (e.g., Lei et al., 2017; Lei et al. 2019b; Sun et al., 2017). Furthermore, we cannot rule out the possibility that, in the Changning source area, the fluids could be from the upper mantle. The Changning mainshock is situated in eastern Tibet, under which there is a BMW structure (e.g., Lei et al., 2009; Lei et al. 2019a; Lei and Zhao, 2016). Under the Burma arc, the Indian plate has subducted down to the mantle transition zone, and in the mantle transition zone it moved northward to the Kunlunshan fault zone and eastward to the Xiaojiang fault zone, which formed the BMW structure (e.g., Lei and Zhao, 2016; Lei et al. 2019a). This result has been supported by the receiver function analyses that show the thickened mantle transition zone in the similar area (e.g., Hu et al., 2013; Shen et al., 2011). In the BMW structure, there exists the hot and wet mantle upwelling due to the dehydration of stagnant plate in the mantle transition zone, due to a large amount of wet sedimentary materials being dragged down to the mantle transition zone by the subducting plate (Regenauer-Lieb et al., 2001) and/or the corner flow caused by the subduction of the Indian plate (Lei et al., 2009; Lei et al. 2019a). Similarly, the 1995 Kobe earthquake could be related to the dehydration of the oceanic crust on the top of the subducting Philippine Sea plate at 50–60 km depth (Zhao et al., 1996). The 1976 Tangshan and 1668 Tancheng earthquakes might be associated with the hot and wet mantle upwelling in the BMW structure formed by the westward deep subduction of the Pacific plate down to the mantle transition zone under eastern China (e.g., Lei and Zhao, 2005, 2006; Lei et al., 2008; Lei et al., 2020).

It should be noted that both low Vp and low Vs velocity discontinuities are observed at depths of 10–15 km along cross section CC' (Fig. 9), which match well with the detachment layer geometrically by previous seismic sounding profile in this area (He et al., 2019). Integrating with the well-tie seismic cross-section results (He et al., 2019), our results suggest that the velocity discontinuity is mainly sand-mudstone interbeded with silty-sandstone layers. Such layers have relatively poorly compressive and shearing strength properties, which are mainly characterized by quasi-plastic mechanisms in the deformation processes. The detachment layer could adjust the structure between the upper and lower strata. Simultaneously, the Luobiao swarm with small earthquakes preferentially occurred within the zones around low-Vp and high-Vs zones at depths of 2–12 km. High-resolution velocity models and precisely relocated earthquakes indicate that the occurrence of small earthquakes is also well correlated with structural variations. Similarly, the source area of the Changning, Gongxian and Xingwen swarms also has such a structural feature (Figs. 7 and 8). Our results suggest that strong structural variations control the structural heterogeneity and the occurrence of the Changning mainshock and its aftershocks.

Last but not least, our precisely relocated earthquakes show that the aftershocks have a multiple-banding distribution in the source area, that is, earthquakes are not restricted to one or more specific tectonic zones (Fig. 6). Some moderate-sized aftershocks ($Ms > 5.0$) are concentrated on the Changning anticline at depths of 5–10 km, where there is a stable pre-Sinian crystalline basement (He et al., 2019). Above these moderate-sized earthquakes, a series of small aftershocks ($Ms < 5.0$) tend to be activated in the shallow crust, due to the upward intrusion of fluids along the anticline and syncline structures in the crust from the upper mantle in the BMW structure. This may explain why many earthquake swarms occurred in the Changning source area. Such a structural feature is well similar to those in the source areas of the 2008 Wenchuan and 1976 Tangshan earthquakes (e.g., Lei et al., 2008; Lei and Zhao, 2009; Xu and Lei, 2020).

5. Conclusions

In this study, we obtain high-resolution Vp, Vs, and Vp/Vs models and precisely relocated earthquakes around the 2019 Changning source area using a number of P- and S-wave arrival times. Our results show that focal depths of the Changning mainshock and its aftershocks are approximately above 10 km, and small earthquakes form a steep dip fault plane. All these earthquakes are underlain by low Vp, low Vs, and high Vp/Vs anomalies, indicating that the fluids could play an important role in enhancing stress concentration in the seismogenic layer of the shallower crust leading to mechanical failure and the nucleation of these earthquakes. These fluids could be associated with the hot and wet mantle upwelling in the BMW formed by the deep subduction of the Indian plate down to the mantle transition zone. A clear velocity discontinuity is observed at ~10–15 km depths beneath the Gongxian and Xingwen swarms, which matches well with the detachment layer by seismic sounding profiles in the region, suggesting that the structural

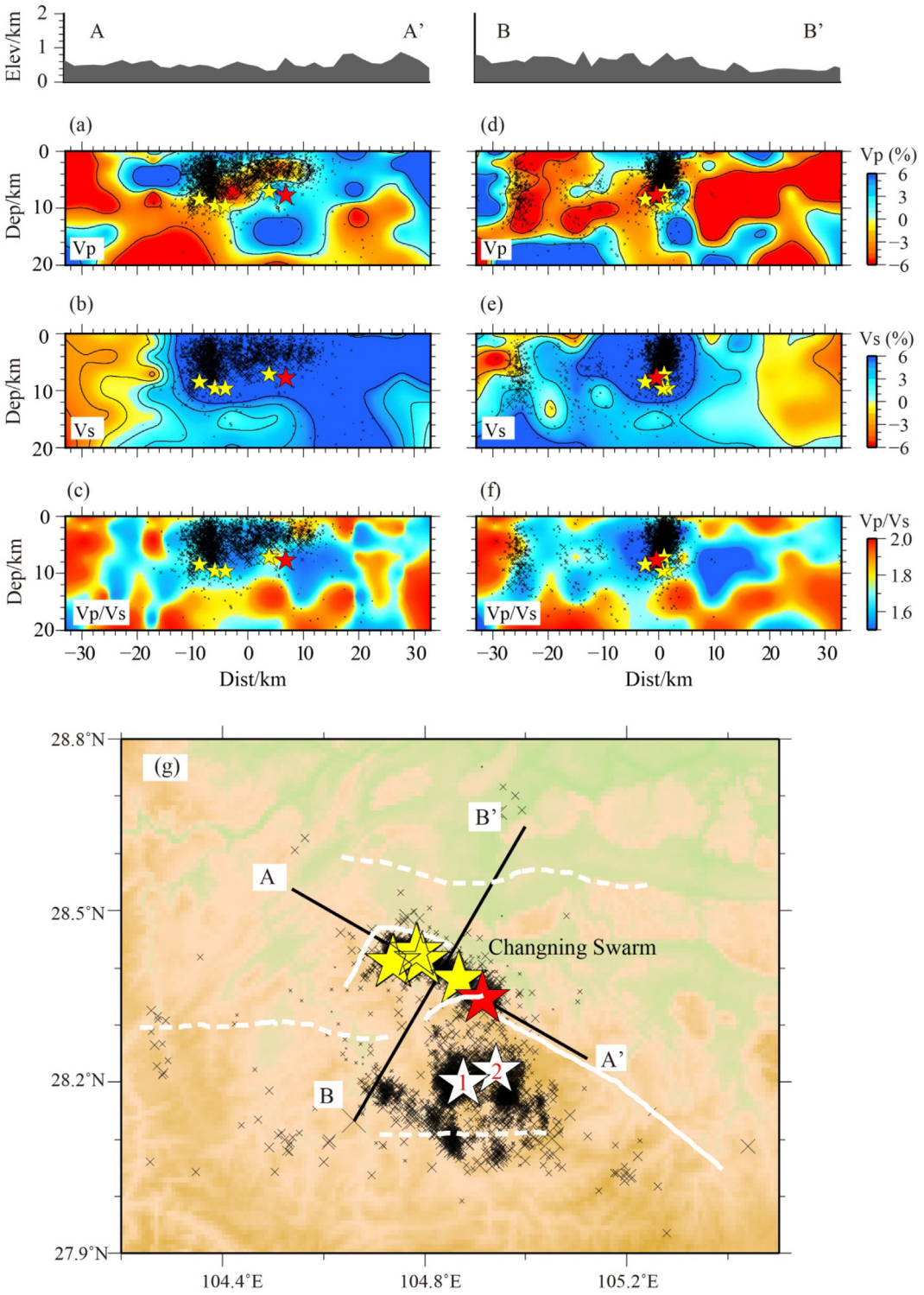

Fig. 7. The same as Fig. 6 but for vertical cross sections passing through the Changning earthquake source area. **(a-c)** Vp, Vs, and Vp/Vs along cross section AA'. **(d-f)** Similar to (a–c) but for cross section BB'. The red color denotes low Vp, low Vs, and high Vp/Vs, respectively, whereas the blue color denotes high Vp, high Vs, and low Vp/Vs, respectively. The color scales for Vp, Vs and Vp/Vs are shown on the right. The surface topography along the cross section is shown on the top. Crosses denote earthquakes that occurred within 5 km off the cross section. **(g)** Location of cross sections. Other symbols are the same as those in Fig. 6. (For interpretation of the references to color in this figure legend, the reader is referred to the web version of this article.)

contrast in the source area could control the generation of the mainshock and the distribution of the aftershock sequences. In addition, a series of small aftershocks above 5–10 km depths could be activated in the shallow crust, due to the upward intrusion of fluids along the anticline and syncline structures in the crust from the upper mantle in the BMW structure.

CRediT authorship contribution statement

Bing Zhang: Methodology, Validation, Formal analysis,

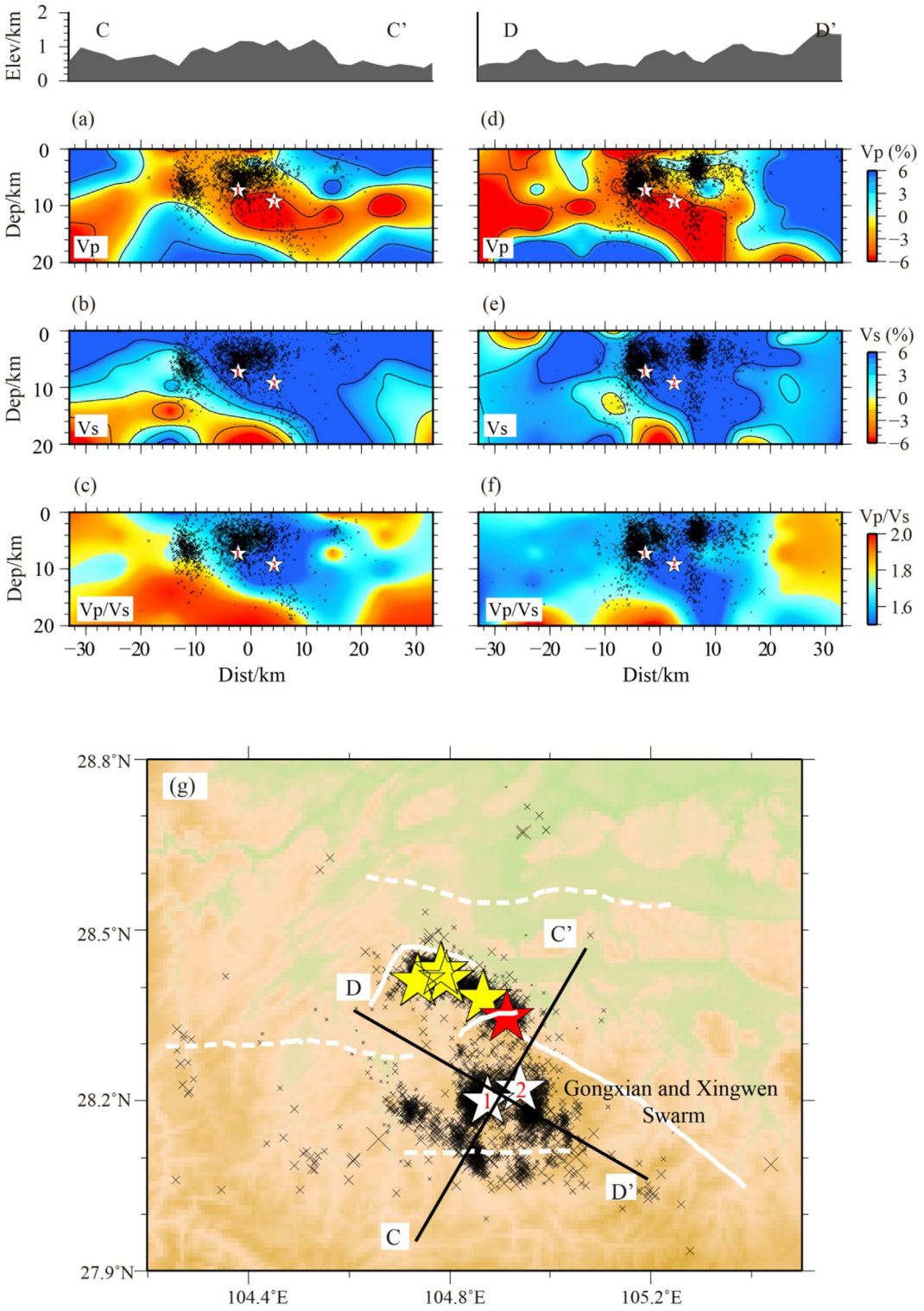

Fig. 8. The same as Fig. 7 but for vertical cross sections CC' and DD' passing through the Gongxian and Xingwen swarms.

Investigation, Writing - original draft, Visualization. **Jianshe Lei:** Conceptualization, Writing - review & editing, Supervision. **Guangwei Zhang:** Methodology, Visualization.

Declaration of Competing Interest

The authors declare that they have no known competing financial interests or personal relationships that could have appeared to influence the work reported in this paper.

Acknowledgements

This work is partially supported by the National Key Research and Development Program of China (2016YFC0600408, 2018YFC1504103) and the National Natural Science Foundation of China (U1939206, 41530212 and 41674091). The seismic waveform data used in this study were provided by the Data Management Centre of the China

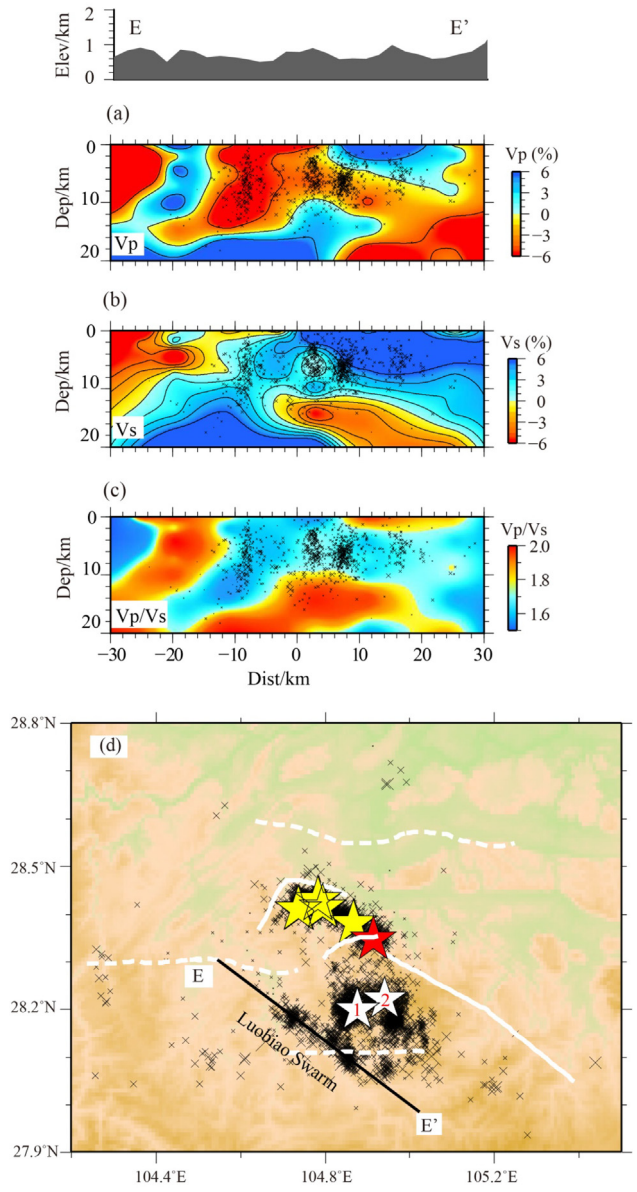

Fig. 9. The same as Fig. 7 but for vertical cross section EE' passing through the Luobiao swarm.

National Seismic Network at the Institute of Geophysics (doi:10.11998/SeisDmc/SN) (Zheng et al., 2010), CEA. The GMT software package distributed by Wessel and Smith (1995) is used for making the figures. Professor Mei-Fu Zhou (the Editor) and an anonymous referee provided thoughtful review comments and suggestions that have improved this paper.

Appendix A. Supplementary material

Supplementary data to this article can be found online at https://doi.org/10.1016/j.jseaes.2020.104492.

References

Bruhn, R., Schultz, R., 1996. Geometry and slip distribution in normal fault systems: Implications for mechanics and fault-related hazards. J. Geophys. Res. 101, 3401–3412.

Deng, Q., Zhang, P., Ran, Y., Yang, X., Mi, W., Chu, Q., 2002. General characteristics of China active tectonics. Sci. China (Ser. D) 32 (12), 1021–1030.

Deng, W., Chen, J., Guo, B., Liu, Q., Li, S., Li, L., Yin, X., Qi, S., 2014. Fine velocity structure of the Longmenshan fault zone by double-difference tomography. Chinese J. Geophys. (in Chinese) 57 (4), 1101–1110.

Fan, C., Li, H., Zhong, C., Qin, Q., Hu, D., Zhang, Y., He, S., Zhang, W., 2018. Tectonic fracture stages and evolution model of Longmaxi Formation shale, Dingshan structure. Southeast Sichuan. Acta Petrolei Sinica 39 (4), 379–390.

Fang, L., Wu, J., Liu, J., Cheng, J., Jiang, C., Han, L., Wang, Y., Chen, K., Zhao X., Wu, Z., 2015. Preliminary on the 22 November 2014 Mw 6.1/Ms6.3 Kangding earthquake, western Sichuan, China. Seismol. Res. Lett. 86(6), 1603-1613.

Guo, H., Zhang, H., Froment, B., 2018. Structural control on earthquake behaviors revealed by high-resolution Vp/Vs imaging along the Gofar transform fault, East Pacific Rise. Earth Planet. Sci. Lett. 499, 243–255.

He, D., Li, D., Zhang, G., Zhao, L., Fan, C., Lu, R., Wen, Z., 2011. Formation and evolution of multi-cycle superposed Sichuan Basin. China. Chinese J. Geol. 46 (3), 589–606.

He, D., Lu, R., Huang, H., Wang, X., Jiang, H., Zhang, W., 2019. Tectonic andgeological background of the earthquake hazards in Changning shale gas development zone, Sichuan Basin. SW China. Petroleum Explorat. Develop. 46 (5), 1051–1064.

Hickman, S., Sibson, R., Bruhn, R., 1995. Introduction to special section: Mechanical involvement of fluids in faulting. J. Geophys. Res. 100, 12831–12840.

Hu, J., Yang, H., Li, G., Wen, L., 2013. Seismic signature of the mantle transition zone beneath eastern Tibet and Sichuan Basin. J. Asian Earth Sci. 62, 606–615.

Lei, J., Zhou, H., 2002. 3-D velocity structure of P wave in the upper mantle beneath southwestern China and its adjacent areas. Acta Seismologica Sinica 15 (2), 134–142.

Lei, J., Zhao, D., 2005. P-wave tomography and origin of the Changbai intraplate volcano in Northeast Asia. Tectonophysics 397, 281–295.

Lei, J., Zhao, D., 2006. Global P-wave tomography: on the effect of various mantle and core phases. Phys. Earth Planet. Inter. 154, 44–69.

Lei, J., Zhao, D., 2007. Teleseismic evidence for a subducting break-off slab under Eastern Turkey. Earth Planet. Sci. Lett. 257, 14–28.

Lei, J., Xie, F., Lan, C., Xing, C., Ma, S., 2008. Seismic images under the Beijing region inferred from P and PmP data. Phys. Earth Planet. Inter. 168, 134–146.

Lei, J., Zhao, D., 2009. Structural heterogeneity of the Longmenshan fault zone and the mechanism of the 2008 Wenchuan earthquake (Ms 8.0). Geochem. Geophys. Geosyst. 10 (10), Q10010. https://doi.org/10.1029/2009GC002590.

Lei, J., Zhao, D., Su, Y., 2009. Insight into the origin of the Tengchong intraplate volcano and seismotectonics in southwest China from local and teleseismic data. J. Geophys. Res. Solid Earth 114, B05302. https://doi.org/10.1029/2008JB005881.

Lei, J., Xie, F., Mishra, O.P., Lu, Y., Zhang, G., Li, Y., 2012. The 2011 Yingjiang, China, earthquake: A volcano-related fluid-driven earthquake? Bull. Seismol. Soc. Am. 102 (1), 417–425.

Lei, J., Zhao, D., 2016. Teleseismic P-wave tomography and mantle dynamics beneath Eastern Tibet. Geochem. Geophys. Geosyst. 17, 1861–1884.

Lei, J., Zhang, G., Xie, F., 2014. The 20 April 2013 Lushan, Sichuan, mainshock, and its aftershock sequence: tectonic implications. Earthquake Science 27 (1), 15–25.

Lei, J., Zhao, D., Xu, X., Xu, Y., Du, M., 2019a. Is there a big mantle wedge structure under eastern Tibet? Phys. Earth Planet. Inter. 292, 100–113.

Lei, J., Zhao, D., Xu, X., Du, M., Mi, Q., Lu, M., 2020. P-wave upper-mantle tomography of the Tanlu fault zone in eastern China. Phys. Earth Planet. Inter. 299, 106402.

Lei, X., Huang, D., Su, J., Jiang, G., Wang, X., Wang, H., Guo, X., 2017. Fault reactivation and earthquakes with magnitudes of up to Mw 4.7 induced by shale-gas hydraulic fracturing in Sichuan Basin. China. Scientific reports 7 (1), 7971.

Lei, X., Wang, Z., Su, J., 2019. The December 2018 ML 5.7 and January 2019 ML 5.3 earthquakes in south Sichuan basin induced by shale gas hydraulic fracturing. Seismol. Res. Lett. 90(3), 1099-1110.

Liang, S., Lei, J., Xu, Z., Xu, X., Zou, L., Liu, J., Chen, H., 2018. Relocation of aftershocks of the 2017 Jiuzhaigou, Sichuan, Ms 7.0 earthquake and inversion for focal mechanism of the mainshock. Chinese. J. Geophys. 61 (5), 2163–2175.

Liang, S., Xu, Z., Sheng, S., Zhang, G., Zhao, B., Zou, L., 2020. Focal mechanism solutions and its stress field of the 2019 Changning, Sichuan mainshock and its moderate-strong aftershocks (Ms ≥ 4.0). Seismology and Geology under review.

Long, F., Zhang, Z., Qi, Y., Liang, M., Ruan, X., Wu, W., Jiang, G., Zhou, L., 2020. Three dimensional velocity structure and accurate earthquake location in Changning-Gongxian area of southeast Sichuan. Earth Planet. Phys. 4 (2), 1–15.

Mishra, O.P., Zhao, D., 2003. Crack density, saturation rate and porosity at the 2001Bhuj, India, earthquake hypocenter: a fluid-driven earthquake? Earth Planet. Sci. Lett. 21, 393–405.

Mishra, O.P., Zhao, D., Wang, Z., 2008. The Genesis of the 2001 Bhuj, India Earthquake (Mw 7.6): a Puzzle for Peninsular India? Indian Minerals 61 (3-4), 149-170.

Pei, S., Su, J., Zhang, H., Sun, Y., Tokso, M., Wang, Z., Gao, X., Liu-Zeng, J., He, J., 2010. Three-dimensional seismic velocity structure across the 2008 Wenchuan Ms 8.0 earthquake, Sichuan, China. Tectonophysics 491 (1–4), 211–217.

Regenauer-Lieb, K., Yuen, D., Branlund, J., 2001. The initiation of subduction: criticality by addition of water? Science 294, 578–580.

Royden, L., King, R., Chen, Z., Liu, Y., 1997. Surface deformation and lower crustal flow in eastern Tibet. Science 276, 788–790.

Royden, L., Burchfiel, B., van der Hilst, R., 2008. The geological evolution of the Tibetan plateau. Science 321, 1054–1058.

Shen, X., Mei, X., Zhang, Y., 2011. The crust and upper-mantle structure beneath the Northeastern margin of Tibet. Bull. Seismol. Soc. Am. 101 (6), 2782–2795.

Sibson, R., 1992. Implications of fault-valve behavior for rupture nucleation and recurrence. Tectonophysics 211, 283–293.

Singh, A., Mishra, O., Yadav, R., Kumar, D., 2012. A new insight into crustal heterogeneity beneath the 2001 Bhuj earthquake region of Northwest India and its implications for rupture initiations. J. Asian Earth Sci. 48, 31–42.

Sun, X., Yang, P., Zhang, Z., 2017. A study of earthquakes induced by water injection in the Changning salt mine area. WS China. J. Asian Earth Sci. 136, 102–109.

Tung, S., Katzenstein, K., Masterlark, T., Lei, J., Wauthier, C., Petley, D., 2019. Sensitivities of geodetic source analyses to elastic crust heterogeneity constrained by

seismic tomography for the 2017 Mw 6.5 Jiuzhaigou, China, Earthquake. Seismol. Res. Lett. 90 (5), 1859–1875.
Wang, X., Lü, J., Xie, Z., Long, F., Zhao, X., Zheng, Y., 2015. Focal mechanisms and tectonic stress field in the North-South Seismic Belt of China. Chinese J. Geophys. (in Chinese) 58 (11), 4149–4162.
Wessel, P., Smith, W., 1995. New, improved version of generic mapping tools released. Eos Transactions 79, 47.
Xie, Z., Zheng, Y., Liu, C., Xiong, X., Li, Y., Zheng, X., 2015. Source parameters of the 2014 Ms 6.5 Ludian earthquake sequence and their implication on the seismogenic structure. Seismol. Res. Lett. 86(6), 1614-1621.
Xu, X., Han, Z., Yang, X., Zhang, S., Yu, G., Zhou, B., Li, F., Ma, B., Chen, G., Ran, Y., 2016. Seismotectonic map in China and its adjacent regions (in Chinese). Seismological Press, Beijing.
Xu, X., Lei, J., 2020. Preface to the special issue on Structure and dynamics of the Longmenshan fault zone. J. Asian Earth Sci. 104474.
Yi, G., Long, F., Liang, M., Zhao, M., Wang, S., Gong, Y., Qiao, H., Su, J., 2019. Focal mechanism solutions and seismogenic structure of the 17 June 2019 Ms 6.0 Sichuan Changning earthquake sequence. Chinese J. Geophys. (in Chinese) 62(9), 3432-3447.
Zhang, G., Lei, J., Liang, S., Sun, C., 2014. Relocations and focal mechanism solution of the 3 August 2014 Ludian, Yunnan Ms 6.5 earthquake sequence. Chinese J. Geophys. (in Chinese) 57(9), 3018-3027.
Zhang, H., Thurber, C., 2003. Double-difference tomography: The method and itsapplication to the Hayward fault. California. Bull. Seismol. Soc. Am. 93, 1875–1889.
Zhang, H., Thurber, C., Bedrosian, P., 2009. Joint inversion for Vp, Vs, and Vp/Vs at SAFOD, Parkfield. California. Geochem. Geophys. Geosyst. 10, Q11002. https://doi.org/10.1029/2009GC002709.
Zhao, D., Kanamori, H., Negishi, H., Wiens, D., 1996. Tomography of the source area of the 1995 Kobe earthquake: Evidence for fluids at the hypocenter? Science 274, 1891–1894.
Zhao, D., Mishra, O.P., Sanda, R., 2002. Influence of fluids and magma on earthquakes: Seismological evidence. Phys. Earth Planet. Inter. 132, 249–267.
Zheng, X., Yao, Z., Liang, J., Zheng, J., 2010. The role played and opportunities provided by IGP DMC of China National Seismic Network in Wenchuan earthquake disaster relief and researches. Bull. Seismol. Soc. Am. 100, 2866–2872.